

Turbulent ‘stopping plumes’ and plume pinch-off in uniform surroundings

Athina Kattimeri · Matthew M. Scase

Received: 30 December 2013 / Accepted: 16 September 2014 / Published online: 27 September 2014
© Springer Science+Business Media Dordrecht 2014

Abstract Observations of turbulent convection in the environment are of variously sustained plume-like flows or intermittent thermal-like flows. At different times of the day the prevailing conditions may change and consequently the observed flow regimes may change. Understanding the link between these flows is of practical importance meteorologically, and here we focus our interest upon plume-like regimes that break up to form thermal-like regimes. It has been shown that when a plume rises from a boundary with low conductivity, such as arable land, the inability to maintain a rapid enough supply of buoyancy to the plume source can result in the turbulent base of the plume separating and rising away from the source. This plume ‘pinch-off’ marks the onset of the intermittent thermal-like behavior. The dynamics of turbulent plumes in a uniform environment are explored in order to investigate the phenomenon of plume pinch-off. The special case of a turbulent plume having its source completely removed, a ‘stopping plume’, is considered in particular. The effects of forcing a plume to pinch-off, by rapidly reducing the source buoyancy flux to zero, are shown experimentally. We release saline solution into a tank filled with fresh water generating downward propagating steady turbulent plumes. By rapidly closing the plume nozzle, the plumes are forced to pinch-off. The plumes are then observed to detach from the source and descend into the ambient. The unsteady buoyant region produced after pinch-off, cannot be described by the power-law behavior of either classical plumes or thermals, and so the terminology ‘stopping plume’ (analogous to a ‘starting plume’) is adopted for this type of flow. The propagation of the stopping plume is shown to be approximately linearly dependent on time, and we speculate therefore that the closure of the nozzle introduces some vorticity into the ambient, that may roll up to form a vortex ring dominating the dynamics of the base of a stopping plume.

A. Kattimeri (✉)
Faculty of Engineering, University of Nottingham, Nottingham NG7 2RD, UK
e-mail: akattimeri@yahoo.co.uk

M. M. Scase
School of Mathematical Sciences, University of Nottingham, Nottingham NG7 2RD, UK

Keywords Plume-thermal transition · Turbulent buoyant plumes · Plume pinch-off · Reduced buoyancy flux · Experimental investigation · Turbulent convection

1 Introduction

Many investigations of turbulent thermal convection have reported structures that can be well-approximated by turbulent plumes (see e.g., [4, 11, 21]). Scorer [33] observed that plumes occurred and persisted in certain areas for a long time, for example the deserts of the US where convection is strong. In places of weak convection, such as the UK, Scorer [33] noted that on many occasions, atmospheric convection has a thermal-like structure. Turbulent plumes that persisted for a short period of time before they pinched-off into thermals, were observed by glider pilots and ornithologists. It was seen that dragonflies did not need much wing-flapping to remain airborne during the morning, when continuous plumes were produced from the ground. However in the late afternoon, the amount of wing-flapping was observed to increase when the ambient convection patterns were more intermittent.

Such unsteady thermal convection phenomena have been observed in patterns of high Reynolds number, $Re \gg 10^4$, convection and they play a central role in many atmospheric, oceanographic and geological processes (see e.g., [13, 22]). It is known, for instance, that when solar radiation is absorbed by the Earth's surface during the day, 'hot-spots' can be created due to the differences in the albedo of the ground [1, 23]. Warm buoyant regions are then formed above the 'hot-spots' removing energy from the ground. If the ground is sufficiently convective, then more heat will be supplied to the warm patch by the hot-spot, producing a sustained turbulent plume. However if the thermal conductivity of the ground is low, there will be insufficient heat flux to the warm patch leading to a pinch-off, and the buoyant region will then rise as a thermal [15].

Transitional behavior is also observed in volcanic plumes. Bluth et al. [3] took Ultra-Violet (UV) images of volcanic SO_2 plumes at Fuego, Guatemala, reporting the disruption of a continuous gas plume by intense thermals. By performing thermal infrared retrievals of SO_2 , Stromboli Volcano, Italy, was also seen to erupt in thermals during the evening and in plumes during the afternoon [27]. Small scale Vulcanian eruptions with strongly unsteady behavior have also been observed and modeled at Santiaguito Volcano, Guatemala (e.g., [28, 31]). Other examples of observations of plume-thermal transition include the Earth's core (see e.g., [14]) and the polar regions of the ocean (see e.g., [2, 38]).

Laboratory-scale studies of turbulent plumes have traditionally exploited the fact that turbulent plumes quickly adjust to a 'pure plume balance' [18] independently of their size, meaning that observations from small scale plumes (e.g., rising from the head of a person in a quiescent office) can be scaled up to have physical relevance at very large scales (e.g., volcanic plumes). Unsteady plume behavior has been considered in a number of experimental campaigns. Townsend [35] carried out experiments in an open-topped box with a uniformly heated, low-conductance plate at the bottom and observed thermal-like convection as opposed to plume-like. Howard [16] later showed that when the Rayleigh number exceeds a critical number, an established plume may disconnect from the thermal boundary layer and rise as a thermal. Periodically forced plumes have been investigated experimentally previously by Cetegen [5–7], though the parameter space considered ($Re \leq 1,500$ and primarily in the transitional/laminar range $Re \leq 900$) makes inference about atmospheric scale flows problematic. Step reductions in source buoyancy of a turbulent plume were considered experimentally by Scase et al. [30], however plume pinch-off was not investigated.

The first explanations of the physical processes behind plume-thermal transition were due to Hunt [20] and Hunt et al. [22]. They noted that when the plume source has low thermal conductivity plume pinch-off can occur. When the source thermal conductivity, k , is greater than that of the flow, and the vertical distance over which heat is conducted in the source, $l \propto k^{1/2}$, is greater than the thickness of the source surface, h , so that the horizontal thermal diffusion in the base is smaller than the vertical diffusion, then a plume can be generated above the source surface. If the source thermal conductivity is decreased by increasing h , such that $l \ll h$, the buoyancy flux reaching the solid surface of the source does not balance the buoyancy lost to the growing plume in the fluid near the solid surface. This results in the existence of horizontal pressure gradients, due to the local cooling at the surface caused by the temperature fluctuations, leading to plume pinch-off. Hence, the plume that was propagating before the cut-off of the supply of buoyant fluid, now rises as a thermal.

Motivated by the work of Hunt et al. [22], Scase et al. [29] modeled an unsteady plume with decreasing source strengths. It was shown that while the assumptions on which the model was based held, no separation of plumes to thermals can occur by simply reducing the driving conditions of the source. In particular, it was shown that when the driving source conditions were reduced rapidly from an initially steady high flux to a new steady low flux, the upper region of the plume (further from the source) and the lower region (closest to the source) appear to act like a classical steady pure plume [24]. However the transitional region, in which the plume adjusts between the upper and the lower regions, necks inwards without pinching-off.

In spite of the progress that has been made in the plume-thermal transition, many fundamental questions remain despite the strong motivation to better understand, for example, geophysical convection and convectively-driven mixing. We perform an experimental investigation of the stopping plume that forces the plume to pinch-off by shutting off the plume's source. As will be shown, the observed dynamics of the pinched-off plume are not well-modelled by established plume or thermal scaling laws. We show that the tail of the pinched-off plume rises approximately linearly in time.

1.1 Layout of paper

In Sect. 2, an experimental investigation into the behavior of an unsteady plume in a uniform environment is presented, focusing on the experimental method and technique we use. A steady plume is first created by releasing salt solution into a tank containing fresh water. The plume then obtains an unsteady nature when the plume nozzle is shut. In Sect. 3, the experimental images and results are presented and analysed. It will be demonstrated that after the source buoyancy flux is reduced to zero, by closing the plume nozzle, plume pinch-off is observed. The unsteady plume detaches from its source with its trailing boundary descending approximately linearly in time. However this trailing boundary exhibits different characteristics from both plumes and thermals, and for this reason we refer to it as a stopping plume. Finally, we discuss our results and draw our conclusions from the main outcomes of the present study in Sect. 4.

2 Experimental set up

2.1 Experimental arrangement

Turbulent plume pinch-off and the transition from a pure to a stopping plume (analogous to a 'starting plume' [36,39]) are experimentally examined. A schematic representation of the

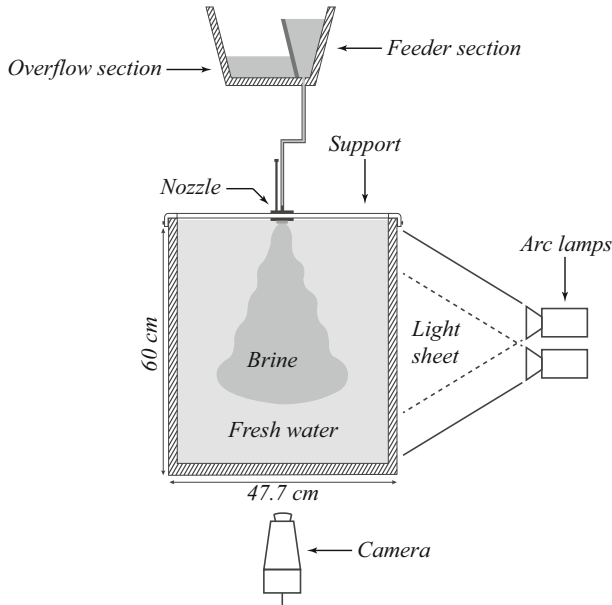


Fig. 1 Sketch of the experimental set-up. The camera view is perpendicular to the light sheet formed by the arc lamps

experimental apparatus is shown in Fig. 1. The experiments were performed in a transparent acrylic tank of dimensions $47.7\text{ cm} \times 47.7\text{ cm}$ in cross-section and 60 cm in height, containing fresh water of relative density 0.998 . The turbulent plume was driven by a constant-head tank, containing brine of relative density 1.068 located above the main tank. We ensured that the two fluids were the same temperature, prior to the start of the experimental process.

The constant-head tank was subdivided into two sections, the feeder section and the overflow section, which were separated by an inclined inner wall. The concentrated salt solution was supplied via transparent tubing, at a steady rate under gravity from the feeder section to a plume nozzle. The nozzle was fixed to a support secured at the top of the tank and submerged just below the free surface of the fresh water, positioned at the center of the tank cross-section for symmetry. The volume of the fluid in the feeder section remained constant at all times in order to ensure that the flow rate through the plume nozzle was constant. This was achieved by constantly pumping fluid from the overflow section into the feeder section, using a submerged pump, at a rate greater than the flow through the plume nozzle, thus maintaining a constant fluid volume in the feeder section and hence pressure head over the plume nozzle.

To achieve the transition to a stopping plume, it was necessary to use a nozzle that could be rapidly closed. At the bottom of the plume nozzle, a rotating control gate was mounted to a metallic rod parallel to the plume nozzle, that could be rotated in order to uncover or cover the nozzle's aperture (of diameter 0.25 cm) without causing significant disturbances in the tank. A turbulent downward plume was induced by rotating the control gate and uncovering the aperture of the nozzle. The rest of the turbulent plume nozzle design was similar to that described in [19].

The plume fluid was marked with Fluorescein dye ($\text{C}_{20}\text{H}_{12}\text{O}_5$). The plume structure was illuminated using a narrow vertical light sheet directed through the center of the plume and produced by two arc lamps. These light sources were mounted one on top of the other and,

in order to prevent light leakage, were positioned inside a box that allowed only a thin light sheet through the experimental tank's side.

The development of the plume's structure was recorded by a digital camera, aligned to view through the side of the main tank and perpendicular to the plane of the light sheet. The digital camera (a NanoSense Mk III) had a $1,280 \times 1,024$ pixel resolution at 8 bits per pixel. Each experiment was performed in a darkened laboratory to improve the overall contrast between plume and ambient fluids.

2.2 Experimental technique

To initiate the experiment, the control gate on the bottom of the nozzle was opened and a downward turbulent starting plume released into the tank. It was necessary to wait until the front of the starting plume was past the camera frame and a steady plume was fully formed, before image capturing began. The rotating gate of the plume nozzle was closed approximately 10 s after the beginning of image capturing. Thereupon the statistically steady plume became a strictly unsteady plume, and plume pinch-off occurred as the source buoyancy flux was reduced rapidly to zero.

Due to the time-dependent and turbulent nature of the flow, a series of experiments was required in order to create an ensemble. Care was taken to ensure that the acquisition time was long enough for the initially released fluid to be regarded as a statistically steady plume in the classical sense, but short enough for the amount of the released fluid not to cause a 'filling box' phenomenon. The images prior to closing the nozzle, were further time-averaged after their ensemble average, resulting in a highly converged representation of the initial steady plume statistics, from which information about the uniformity of the achieved light-sheet could be deduced.

All experimental images were captured and post-processed using DigiFlow [8]. A movie of the ambient fluid prior to any plume flow, was captured and time-averaged to obtain a measure of the background light intensity. The resulting background image was then subtracted from all plume frames, to obtain solely the signal of the plume itself. The dye concentration is linearly proportional to light intensity [37], which in itself is also proportional to the plume's reduced gravity field (cf. [30]). Therefore by subtracting the background image from the ensemble movie of the plume's behavior, we form images providing quantitative information on the plume's reduced gravity.

In order to allow real-world spatial measurements to be acquired from the digital images, a grid comprising an array of squares of known dimension was situated inside the tank and in the light sheet. An image of the grid was then captured. The coordinate points in the mesh were then used as a reference for the linear-mapping procedure, to convert the pixel image coordinates to the physical coordinates.

3 Experimental analysis

3.1 Steady pure plume

Figure 2 illustrates the steady-state plume in uniform quiescent surroundings before the reduction in the source buoyancy flux. Image (a) is a single image from the ensemble-averaged steady plume and image (b) shows the time-averaged ensemble structure of the plume. It is evident that there is a deflection of the vertical axis of the plume near the source due to the design of the gate at the bottom of the nozzle. This asymmetry inhibits entrainment

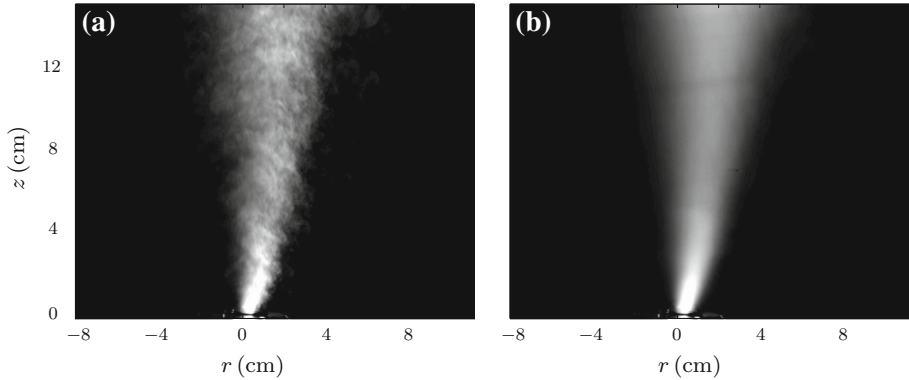
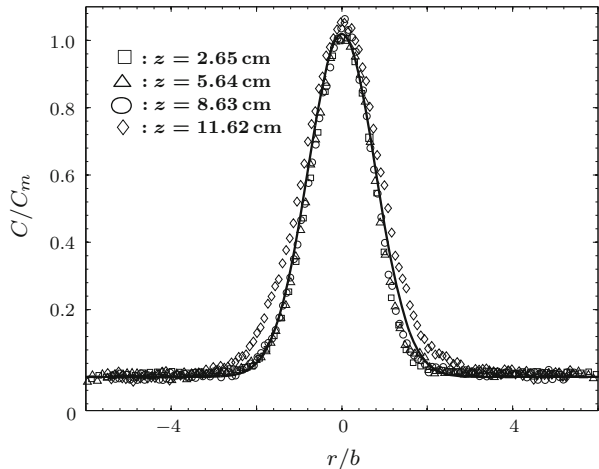


Fig. 2 **a** A raw image of the steady plume. **b** Time-averaged exposure of the steady plume

Fig. 3 Gaussian profile of the passive tracer in different cross-plume regions. The *black line* represents the Gaussian fitting with $A = 1$ and $\mu = 0$. The maximum concentration, C_m , and the plume width, b , were found by taking the logarithm of C and best fitting a quadratic curve



immediately adjacent to the nozzle, forcing the plume horizontally to the right as shown. However approximately 2 cm above the source, as shown, the buoyancy dominates over this initial asymmetry and the plume’s direction of propagation becomes vertical.

The profile of dye concentration is determined using the standard assumption that it is linearly proportional to light intensity. Figure 3 represents the concentration of the passive tracer, C , across the steady initial plume at different heights. As shown, the dye concentration of the plume remains Gaussian implying self-similarity and it can be described by a normal distribution of the form,

$$X(r, z; t) = A(z, t) \exp \left\{ -\frac{[r - \mu(z, t)]^2}{2 \sigma(z, t)^2} \right\}, \tag{1}$$

where $A(z, t)$ is the signal amplitude, $\mu(z, t)$ is the radial location of the signal peak and $\sigma(z, t)$ is the standard deviation. It can be observed that the dye concentration increases towards the centre of the plume. Figure 4a is obtained by fitting a Gaussian of the form (1) to the plume mean structure, at each vertical height.

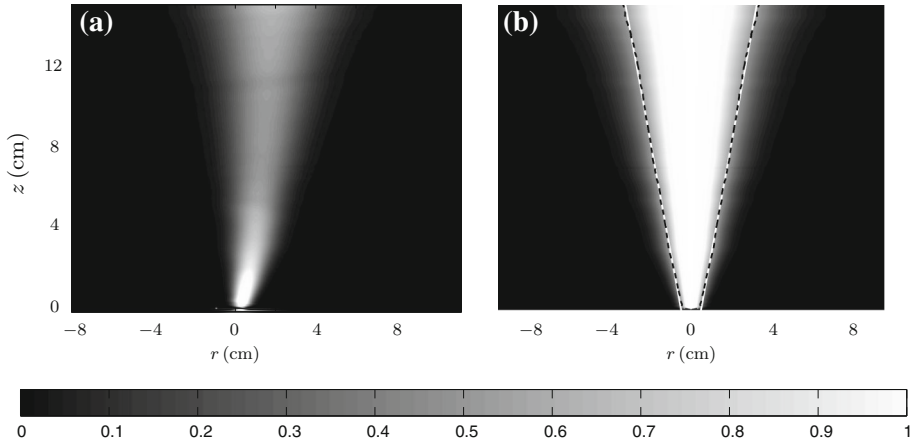


Fig. 4 **a** Image of the Gaussian fitting of the time-averaged plume. **b** Centered image of the plume with scaled concentration, where the *black solid* and *white dashed lines* illustrate the plume envelope. The *colorbar* shows the normalised concentration

Figure 4b shows the straightened vertical steady plume with scaled concentration, achieved by laterally displacing each Gaussian fit until the centre is at $r = 0$ and then re-scaling the plume on its centerline, peak intensity. The lateral displacement technique that we have employed was originally developed by Hübner [17]. The steady envelope of the plume is represented by both the white solid line and the black dashed line. The Gaussian plume width, b , can be defined as the distance from the centerline at $r = 0$ to the point $r = b$ where $X(b, z) = e^{-1} X(0, z)$, and thus $\exp\{-b^2/2\sigma^2\} = \exp\{-1\}$, and so $b = \sqrt{2}\sigma$. The total concentration, C_T , at a specific vertical height and time is found by integrating over the horizontal plane (cf. [30]), and is given by

$$C_T(z, t) = 2\pi A(z, t)\sigma(z, t)^2. \tag{2}$$

Hence by (2), $b = \sqrt{C_T/\pi A}$, and this is illustrated by the dashed black line. The solid white line was produced by best-fitting to the calculated $b(z)$ (dashed black line), to determine the entrainment coefficient, $\alpha = 0.110$, and the virtual origin correction, $b_0 = 0.432$ cm, such that $b = \frac{6\alpha z}{5} + b_0$. The turbulent plume flow is therefore initially confined to a conical region with semi-angle given by $\tan \theta = 0.132$. The measured value of α is consistent with that found in the meta-analysis of Papanicolaou and List [26].

3.2 Stopping plume

In order to initiate plume pinch-off and therefore a stopping plume, the supply of the buoyant fluid in an established steady turbulent plume was cut off. The concentration decreases with the decrease in buoyancy, since the flux of buoyant fluid through the source into the plume is reduced. The unsteady plume continues to entrain ambient fluid becoming more dilute, and thus the plume edges move towards the center tending to disconnect from the source, resulting in plume pinch-off. This type of narrowing behavior of the unsteady plume was also reported in [29,32], though no plume pinch-off was observed there.

At $t = 0$ s, the nozzle is completely closed resulting in the formation of an unsteady region of buoyant plume. Images from an ensemble of 24 nominally identical experiments

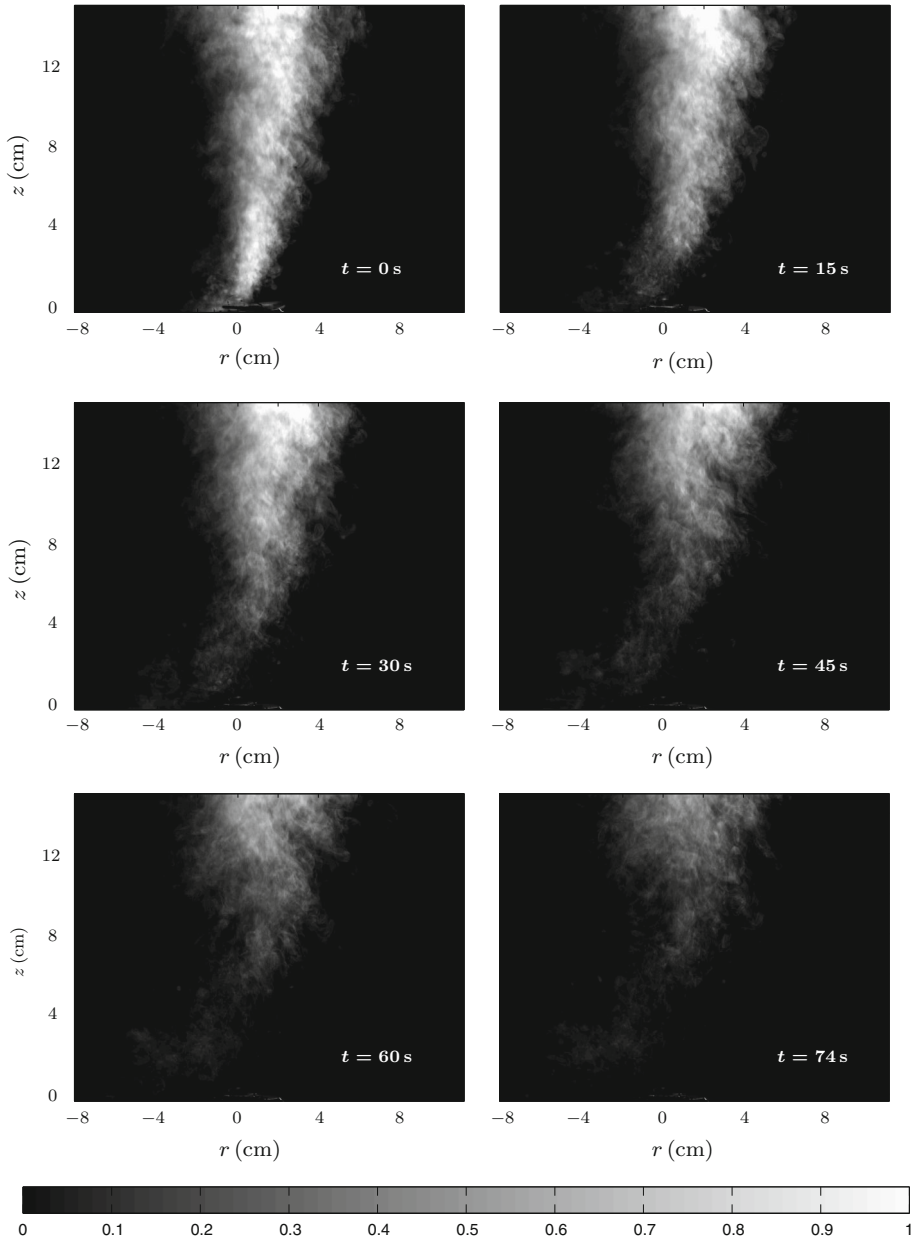


Fig. 5 Individual frames from an ensemble realisation of the stopping plume. The bar underneath specifies the light intensity

are shown in Fig. 5. The ensemble profile changes as time evolves and the base of the plume is seen to move away from the source.

Figure 6 shows the concentration of the passive tracer, C , across the plume for different vertical heights and times corresponding to the frames shown in Fig. 5. As shown, the dye

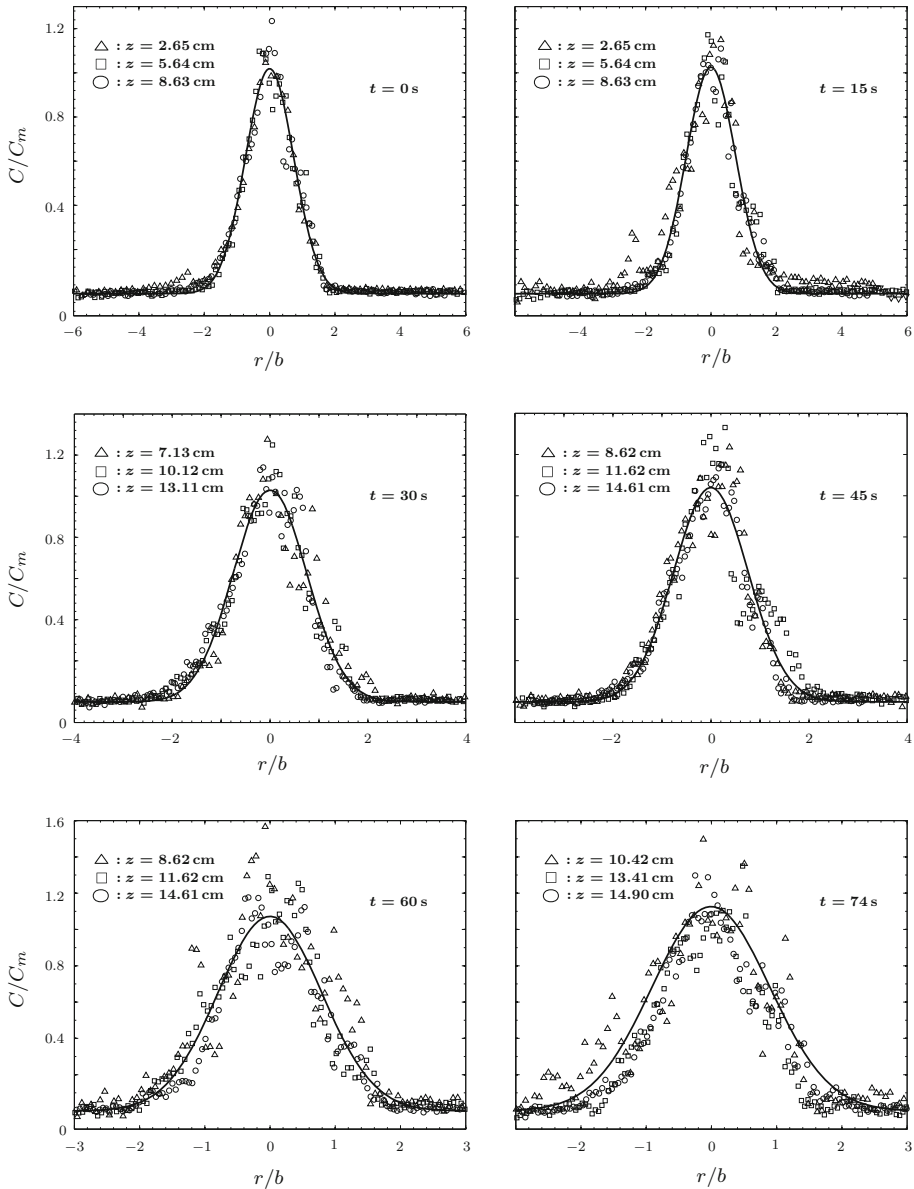


Fig. 6 A plot of the temporal variation of the plume concentration (light intensity) against the radial distance. The black solid line represents the Gaussian fitting with $A = 1$ and $\mu = 0$. The maximum concentration, C_m , and the plume width, b , were found by taking the logarithm of C and best fitting a quadratic curve

concentration of the plume remains approximately Gaussian and can therefore be well-described by (1).

Since C is proportional to reduced gravity, g' , it can be concluded that the buoyancy profile should also be Gaussian. The values of the vertical heights displayed in the images were chosen to represent horizontal sections of the lower, middle and upper regions of the

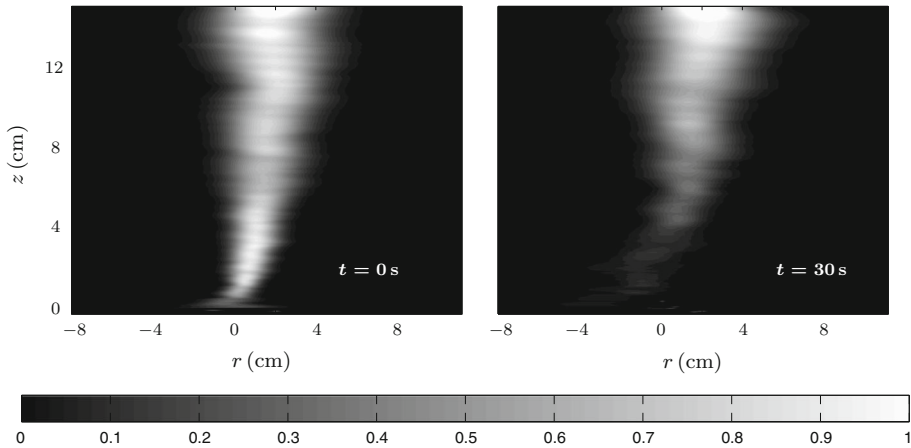


Fig. 7 Plots of the time-dependent plume for $t = 0, 30$ s after undertaking a Gaussian fitting. The normalised light intensity values are given by the *color bar*

plume at a specific time. It can be observed that in the final images, for $t = 60$ and 74 s, the tracer concentration begins to lose its self-similar Gaussian form as the plume nears its total dilution into the ambient.

A Gaussian fit at each height and time was performed on all ensemble averaged experimental images, since the unsteady flow at each height can be described by the distribution curve given in (1). Figure 7 illustrates the ensemble-averaged plume for two specific times after undertaking a Gaussian fitting. The normalized ensemble-averaged plume shown in Fig. 8, was firstly shifted horizontally at each height to align the plume centrally. Then the spatial variation of the light-sheet was corrected for, by using the centerline values of the initial steady plume.

Figure 8 shows the transition from a steady plume to a stopping plume. In all images the unsteady envelope (black line) is a contiguous, non-isolated, contoured threshold, chosen to be 0.4, giving agreement with the $e^{-1} = X(b, z)/X(0, z)$ standard definition of the plume edge. We take the lowest point of this contour to define the plume base, $z_p(t)$ (indicated by a white circle), though, as with the plume edge, plume fluid may exist outside this contour (as indeed may isolated closed contours). At $t = 0$ s, $z_p = 0$ cm as the plume edges meet to create a ‘pinch-off’. After the control gate is completely closed at $t = 0$ s, the plume detaches from the source. The plume then rises into the surrounding fluid traveling away from the source. After time $t = 74$ s, the region originally occupied by the plume fluid is largely diluted into the ambient fluid.

The variation with time, t , of the position of the base of the plume, z_p , is shown in Fig. 9 for three values of concentration contour, $C = 0.3, 0.4, 0.45$. This range of concentration values spans the standard definitions of plume width, and all exhibit an approximately linear behaviour. The solid data points corresponding to $C = 0.4$, have a best fit line $z_p = 0.157 t$ indicated by the solid line. The open data points corresponding to $C = 0.3$ (squares) and $C = 0.45$ (circles), have dashed best fit lines $z_p = 0.138 t$ and $z_p = 0.163 t$, respectively. The best fit lines through the data therefore indicate that

$$z_p = (0.16 \pm 0.02) t, \tag{3}$$

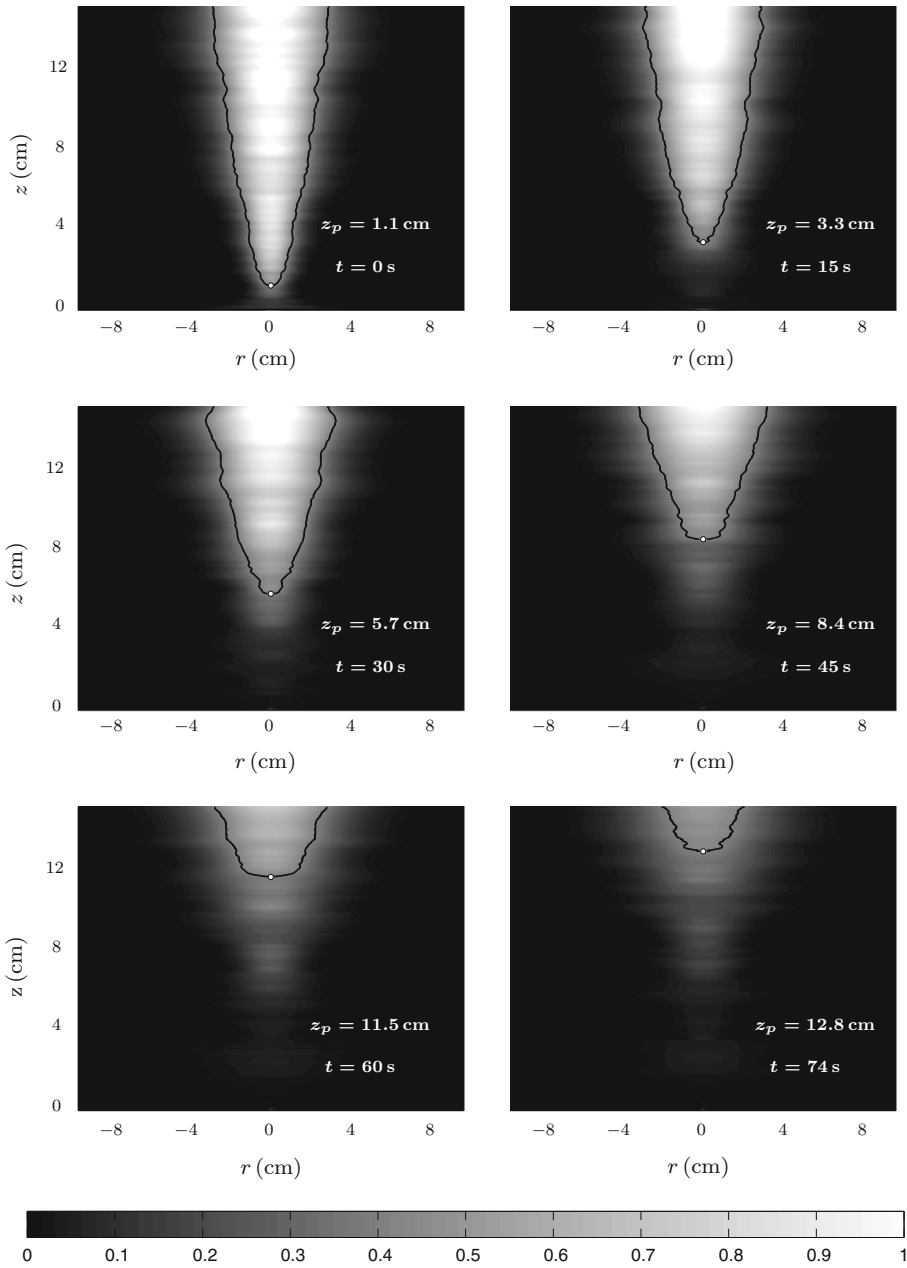


Fig. 8 Centered plume images with scaled concentration for different times. The plume envelope and the position of the plume’s rear, z_p , are indicated by the *black solid line* and the *white small circle*, respectively. The *bar* underneath indicates the normalised light intensity

is a reasonable approximation to the position of the base of the plume, for the parameters in the present experimental arrangement. We note that a different scaling behavior for the stopping plume is being observed compared to standard plume and thermal models, as neither

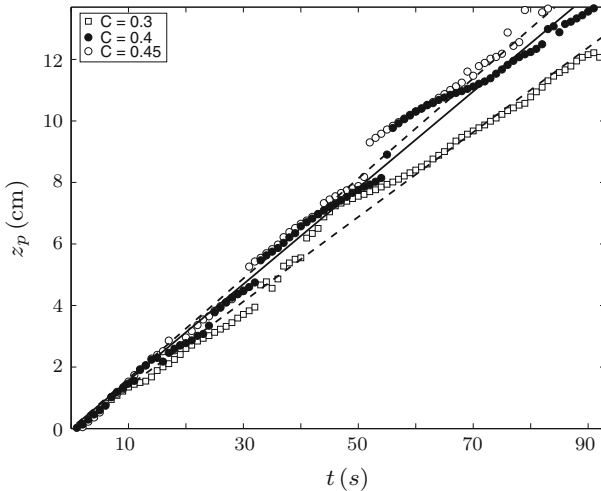


Fig. 9 The variation of the position of the base of the stopping plume, z_p , with time, t . The solid data points are experimental measurements taken at a concentration $C = 0.4$, and the *solid line* is a linear best fit with a positive gradient of 0.16 cm s^{-1} . The open data points demonstrate that the observed linear behavior is not dependent on the choice of C , and cover a range that includes the standard $C = 1/e \approx 0.37$ value. *Dashed lines* are best fits to the open data points. It can be observed that the ascent of the stopping plume is approximately linearly proportional to time. The steps in the data are non-physical and are an artefact of the contouring algorithm

the position of a fluid parcel in a steady plume, nor the propagation of a thermal are linearly proportional to time.

It is apparent that there are steps in the data (e.g., at $t \approx 55 \text{ s}$). These are non-physical and occur as a result of the contouring of the experimental images. One consequence of the span-wise only Gaussian fitting is that some horizontal banding appears in the post-processed experimental images (see e.g., Fig. 8). Contouring for a specific intensity value, and in particular focussing on the approximately horizontal portion of those contours, is especially sensitive to the banding. Nevertheless, while the step-like upward fluctuations in the calculated position of z_p are unphysical, the mean path through the data points is an accurate representation of the propagation of the base of the plume.

3.3 The base of a stopping plume

The results of Sects. 3.1 and 3.2 allow us to give a first tentative description of the behavior of stopping plumes. The scaling law (3) indicates that the behavior of plumes and thermals are different to the behavior of the stopping plume observed in our experiment (see Figs. 5, 6, 7, 8). We recall that the vertical position of a thermal scales as $t^{1/2}$ [34] since,

$$\frac{\partial z}{\partial t} = w = c_0 z^{-1/2} \Rightarrow z \propto t^{1/2}, \tag{4}$$

for some constant c_0 , and that the vertical height of a plume scales as $t^{3/4}$ [24] since,

$$\frac{\partial z}{\partial t} = w = c_1 z^{-1/3} \Rightarrow z \propto t^{3/4}, \tag{5}$$

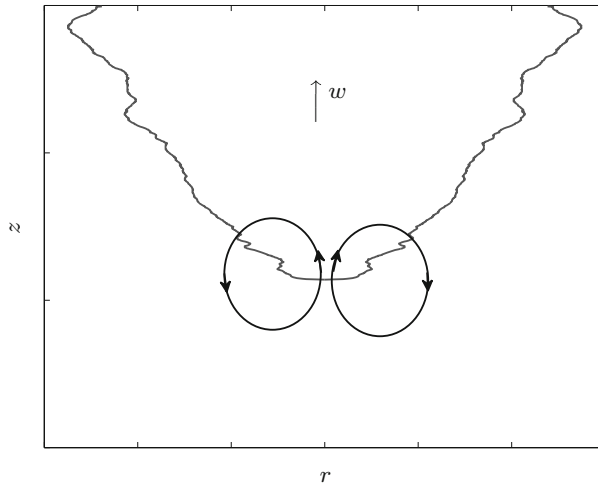


Fig. 10 Schematic representation of the vortex rings (when hypothesizing their existence) at the bottom of the stopping plume. The *black circles* indicate the conjectured structure of the vortex ring and the *arrows* point their flow motion

for some constant c_1 . In contrast, the linear dependence on time of the propagation of the base of the stopping plume lies outside the range of the power law behavior of plumes and thermals indicated in (4) and (5). So we propose that the stopping plume may not be regarded in some sense as a ‘hybrid’ plume/thermal—some new dynamics must be involved. It is possible that as the established steady plume is forced to stop, a new flow is induced in the ambient.

One possible explanation would be that as the stopping plume rises away from the nozzle, a shear flow is induced near the boundary of the source introducing new vorticity into the ambient. The roll-up of the vorticity into a vortex ring may then control the dynamics at the base of the stopping plume (see Fig. 10) if the shear is strong enough. The family of vortex rings studied by Norbury [25], which includes thin-cored rings [9, 10] and Hill’s spherical vortex ring [12], all propagate steadily. Hence we might anticipate that if an induced vortex ring approximates a member of this vortex ring family, then the propagation of the base of the stopping plume may be linear in time.

4 Discussion and conclusions

Systems of high Reynolds number convection have been observed to transition between plume-dominated and thermal-dominated regimes. Motivated by the work of Hunt et al. [22], the present study aimed to obtain a better understanding of the dynamics of the plume-thermal transition. Improved accuracy in the modeling of plumes is desirable as large scale weather and ocean models, with grid sizes on the order of between 100 m and 1 km, are unable to resolve them accurately and yet they provide a key source of forcing, for example the dense bottom waters that travel down the continental slopes of Antarctica that play a key role in driving ocean circulation.

Our experimental investigation showed that for the parameters considered, plume pinch-off resulted in the formation of what we have termed a ‘stopping plume’—an individual buoyant fluid region detached from the source and propagating into the ambient. The light

intensity (proportional to the concentration of the passive tracer and therefore the reduced gravity field), was shown to exhibit a Gaussian profile across all heights at all times to a good approximation. The propagation behavior of the stopping plume behaved neither as a plume nor as a thermal, as the position of the base of the stopping plume traveled approximately linearly in time. We have therefore suggested that some extra dynamics, not captured by the experimental visualization, may be responsible for this behavior and we believe, it is plausible to suggest that a vortex ring may be induced at the base of the stopping plume.

We have chosen to refer to the investigated flow as a ‘stopping plume’ by analogy with Turner’s [36] ‘starting plume’. The front of the starting plume was modeled as a turbulent vortex ring, and the scaling law observed in our experiments indicates that the stopping plume may be controlled by a vortex ring too. The starting plume propagates into a quiescent, vorticity-free ambient fluid and so does not induce any extra flow in the ambient beyond the standard entrainment into a turbulent plume. Conversely, we are suggesting that in the process of pinching-off, the stopping plume does induce vorticity into the ambient. Previous investigations have considered the effect of ambient vorticity on the behavior of plumes. Indeed Witham and Phillips [40] showed that the top of a turbulent plume could be made to pinch-off as a result of detrainment due to turbulence in the ambient, but they did not observe a transition from plume-like to thermal-like behavior such as has been forced here. There exists the possibility that a combination of turbulent detrainment and source weakening may be responsible for plume pinch-off in atmospheric flows, though here we have considered only source weakening.

Acknowledgments AK acknowledges support from Engineering and Physical Sciences Research Council (EPSRC) studentship. AK and MMS would like to gratefully acknowledge the very constructive input of the Referees.

References

1. Ahrens CD (2000) Essentials of meteorology: an invitation to the atmosphere. Cengage Learning, Stamford
2. Backhaus JO, Kampf J (1999) Simulations of sub-mesoscale oceanic convection and ice–ocean interactions in the Greenland sea. *Deep-Sea Res II* 46:1427–1455
3. Bluth GJS, Shannon JM, Watson IM, Prata AJ, Realmuto VJ (2007) Development of an ultra-violet digital camera for volcanic SO₂ imaging. *J Volcanol Geotherm Res* 161:47–56
4. Castaing B, Gunaratne G, Heslot F, Kadanoff L, Libchaber A, Thomae S, Wu XZ, Zaleski S, Zanetti G (1989) Scaling of hard thermal turbulence in Rayleigh–Bénard convection. *J Fluid Mech* 204:1–30
5. Cetegen BM, Ahmed TA (1993) Experiments on the periodic instability of buoyant plumes and pool fires. *Combust Flame* 93:157–184
6. Cetegen BM, Kasper KD (1997) Experiments on the oscillatory behaviour of buoyant plumes of helium and helium–air mixtures. *Phys Fluids* 8:2974–2984
7. Cetegen BM (1997) Behavior of naturally unstable and periodically forced axisymmetric buoyant plumes of helium and helium–air mixtures. *Phys Fluids* 9:3742–3752
8. Dalziel SB (2012) DigiFlow. DL Research Partners. <http://www.damtp.cam.ac.uk/lab/digiflow>
9. Fraenkel LE (1970) On steady vortex rings of small cross-section in an ideal fluid. *Proc R Soc A* 316:29–62
10. Fraenkel LE (1972) Examples of steady vortex rings of small cross-section in an ideal fluid. *J Fluid Mech* 51:119–135
11. Grossmann S, Lohse D (2000) Scaling in thermal convection: a unifying theory. *J Fluid Mech* 407:27–56
12. Hill MJM (1894) On a spherical vortex. *Phil Trans R Soc Lond A* 185:231–245
13. Holland PR, Hewitt RE, Scase MM (2014) Wave breaking in dense plumes. *J Phys Oceanogr* 44:790–800
14. Hollerback R, Jones CA (1993) Influence of the earth’s inner core on geomagnetic fluctuations and reversals. *Nature* 365:541–543
15. Horsch GM, Stefan HG (1988) Convective circulation in littoral water due to surface cooling. *Limnol Oceanogr* 33:1068–1083

16. Howard LN (1964) Convection at high Rayleigh number. In: Gortler H (ed) Proceedings 11th international congress on applied mechanics. Springer, Munich, pp 1109–1115
17. Hübner J (2004) Buoyant plumes in a turbulent environment. PhD Thesis. University of Cambridge
18. Hunt GR, Kaye NB (2005) Lazy plumes. *J Fluid Mech* 533:329–338
19. Hunt GR, Linden PF (2001) Steady-state flows in an enclosure ventilated by buoyancy forces assisted by wind. *J Fluid Mech* 426:355–386
20. Hunt JCR (1998) Eddy dynamics and kinematics of convective turbulence. In: Plate EJ, Fedorovich E (eds) Buoyant convection in geophysical flows. Kluwer, Dordrecht, pp 41–82
21. Hunt JCR, Kaimal JC, Gaynor JE (1988) Eddy structure in the convective boundary layer—new measurements and new concepts. *Q J R Met Soc* 114:827–858
22. Hunt JCR, Vrieling AJ, Nieuwstadt FTM, Fernando HJS (2003) The influence of the thermal diffusivity of the lower boundary on eddy motion in convection. *J Fluid Mech* 491:183–205
23. Lei C, Patterson JC (2002) Natural convection in a reservoir sidearm subject to solar radiation: experimental observations. *Exp Fluids* 32:590–599
24. Morton BR, Taylor GI, Turner JS (1956) Turbulent gravitational convection from maintained and instantaneous sources. *Proc R Soc Lond A* 234:1–32
25. Norbury J (1972) A family of steady vortex rings. *J Fluid Mech* 57:417–431
26. Papanicolaou PN, List EJ (1988) Investigations of round vertical turbulent buoyant jets. *J Fluid Mech* 195:341–391
27. Prata AJ, Bernardo C (2008) Retrieval of SO₂ from a ground-based thermal infrared imaging camera. NILU internal report
28. Rose WI (1987) Volcanic activity at Santiaguito Volcano, 1976–1984. *Spec Pap Geol Soc Am* 212:101–111
29. Scase MM, Caulfield CP, Dalziel SB, Hunt JCR (2006) Time-dependent plumes and jets with decreasing source strengths. *J Fluid Mech* 563:443–461
30. Scase MM, Caulfield CP, Dalziel SB (2008) Temporal variation of non-ideal plumes with sudden reductions in buoyancy flux. *J Fluid Mech* 600:181–199
31. Scase MM (2009) Evolution of volcanic eruption columns. *J Geophys Res* 114:F04003
32. Scase MM, Hewitt RE (2012) Unsteady turbulent plume models. *J Fluid Mech* 697:455–480
33. Scorer RS (1954) The nature of convection as revealed by soaring birds and dragonflies. *Q J R Met Soc* 80:68–77
34. Scorer RS (1957) Experiments on convection of isolated masses of buoyant fluid. *J Fluid Mech* 2:583–594
35. Townsend AA (1959) Temperature fluctuations over a heated horizontal surface. *J Fluid Mech* 5:209–241
36. Turner JS (1962) The ‘starting plume’ in neutral surroundings. *J Fluid Mech* 13:356–368
37. Unger DR, Muzzio FJ (1999) Laser-induced fluorescence technique for the quantification of mixing in impinging jets. *AIChE J* 45:2477–2486
38. Uscinski BJ, Kaletsky A, Stanek CJ, Rouseff D (2003) An acoustic shadowgraph trial to detect convection in the arctic. *Waves Random Media* 13:107–123
39. Wang RQ, Law AWK, Adams EE, Fringer OB (2011) Large-eddy simulation of starting buoyant jets. *Environ Fluid Mech* 11:591–609
40. Witham F, Phillips JC (2008) The dynamics and mixing of turbulent plumes in a turbulently convecting environment. *J Fluid Mech* 602:39–61